RSC Advances

PAPER

View Article Online
View Journal | View Issue

Cite this: *RSC Adv.*, 2019, **9**, 27500

Reinforced anion exchange membrane based on thermal cross-linking method with outstanding cell performance for reverse electrodialysis†

Young Ju Lee,[a] Min Suc Cha,[ab] Seong-Geun Oh,[b] Soonyong So,[a] Tae-Ho Kim,[a] Won Sun Ryoo,*[c] Young Taik Hong[a] and Jang Yong Lee*[a]

Received 2nd July 2019
Accepted 26th August 2019

DOI: 10.1039/c9ra04984c

rsc.li/rsc-advances

A poly(ethylene)-reinforced anion exchange membrane based on cross-linked quaternary-aminated polystyrene and quaternary-aminated poly(phenylene oxide) was developed for reverse electrodialysis. Although reverse electrodialysis is a clean and renewable energy generation system, the low power output and high membrane cost are serious obstacles to its commercialization. Herein, to lower the membrane cost, inexpensive polystyrene and poly(phenylene oxide) were used as ionomer backbones. The ionomers were impregnated into a poly(ethylene) matrix supporter and were cross-linked *in situ* to enhance the mechanical and chemical properties. Pre-treatment of the porous PE matrix membrane with atmospheric plasma increased the compatibility between the ionomer and matrix membrane. The fabricated membranes showed outstanding physical, chemical, and electrochemical properties. The area resistance of the fabricated membranes (0.69–1.67 Ω cm^2) was lower than that of AMV (2.58 Ω cm^2). Moreover, the transport number of PErC(5)QPS-QPPO was comparable to that of AMV, despite the thinness (51 μm) of the former. The RED stack with the PErC(5)QPS-QPPO membrane provided an excellent maximum power density of 1.82 W m^{-2} at a flow rate of 100 mL min^{-1}, which is 20.7% higher than that (1.50 W m^{-2}) of the RED stack with the AMV membrane.

1. Introduction

Recently, renewable energy sources such as solar, wind, biomass, and salinity gradient energy have gained significant attention as the ultimate solutions to the depletion of fossil fuels and environmental pollution. Among various energy conversion technologies based on sustainable energy sources, reverse electrodialysis (RED) has received attention as a promising non-polluting, sustainable technology because of its advantages, such as being an unlimited and clean energy source with a simple system configuration and moderate system cost.[1–5]

RED is an energy conversion system that converts the Gibbs free energy from mixing saline water and fresh water to electrical energy. The RED stack consists of a number of single cells composed of an end plate, electrode, spacer, and redox couple that converts chemical energy to electrical energy, and two kinds of ion exchange membranes (IEMs), *i.e.*, a cation exchange membrane (CEM) that is permeable to positive ions and an anion exchange membrane (AEM) that is only permeable to negative ions.[6–10] The compartments separated by membranes are alternately filled with a concentrated salt solution and a dilute salt solution. The salinity gradient leads to a potential difference over each membrane, the so-called membrane potential. The ions are transported from the concentrated salt solution to the dilute salt solution through each membrane by the chemical potential difference; that is, cations permeate through the CEM in the direction of the cathode, and anions permeate through the AEM in the direction of the anode. The ionic flux gives rise to an ionic current that is converted to an electrical current at the electrodes by the redox reaction of proper redox couples. Typically, in the RED system, the IEM determines the system performance as well as the system cost. A number of studies on CEMs have been conducted over the past several decades, whereas studies on AEMs are relatively few, regardless of the criticality, because of the high level of technical difficulty. Although reinforced membranes with hydrocarbon-based AEMs (such as AMX and AMV), which show outstanding cell performance, have been used in RED systems, their high membrane cost is regarded as the major obstacle to their use in RED technology. Thus, the development of alternate membranes with outstanding cell performance, excellent chemical stability, and reasonable cost has been considered as the most significant task for a commercialization of REDs.[11,12] As shown in previous studies, polystyrene (PS) and

[a]*Center for Membrane, Korea Research Institute of Chemical Technology, 141 Gajeong-ro, Yuseong-gu, Daejeon 34114, Republic of Korea*

[b]*Department of Chemical Engineering, Hanyang University, 222 Wangsimni-ro, Seongdong-gu, Seoul 04763, Republic of Korea*

[c]*Department of Chemical Engineering, Hongik University, 94 Wausan-ro, Mapo-gu, Seoul 04066, Republic of Korea*

† Electronic supplementary information (ESI) available. See DOI: 10.1039/c9ra04984c

poly(phenylene oxide) (PPO) have been widely used as matrix polymers for the synthesis of hydrocarbon-based ionomers because of their low cost, good mechanical properties, and easy processibility.[4,13–21] PS and PPO are easily converted to chloromethylated PS (cmPS) and brominated PPO (brPPO), which are precursor polymers of quaternary-aminated PS (QPS) and quaternary-aminated PPO (QPPO), respectively. However, after the quaternization reaction of cmPS and brPPO, QPS and QPPO showed lower mechanical and chemical stability due to increased water uptake; thus, QPS and QPPO are typically used in the cross-linked ionomer form. In other words, QPS and QPPO are not appropriate polymer materials for fabrication and use in the film form because QPS and QPPO are too brittle and soft, respectively, despite the introduction of ion exchange groups. In particular, the dimensional stability of non-crosslinked QPPO is too poor to facilitate its standalone use due to the flexible backbone structure. Therefore, cross-linking between QPS and QPPO is expected to be an effective method for producing an AEM with a reasonable price and outstanding properties for RED, because this method can permit adjustment of the balance between the physical and electrochemical properties.[17,22–27]

In this study, an AEM, *i.e.*, a poly(ethylene) (PE)-reinforced membrane based on cross-linked QPS-QPPO, is reported for RED application. In our previous study, a simple cross-linking method using a primary diamine-based cross-linker to improve mechanical and chemical stability of an AEM was reported.[5,12,28] Primary diamine-based cross-linkers are considered more effective materials than tertiary diamine-based cross-linkers as the cross-linker acts only as a cross-linker without increasing the ion exchange capacity (IEC). The degree of cross-linking is optimized herein to achieve a high quality membrane by varying the amount of cross-linker. Moreover, the reinforced membrane intended for impregnation with C($100x'/x$)QPS-QPPO in a porous polyethylene (PE) matrix membrane is fabricated to maximize the mechanical and chemical properties of the membrane. The porous PE matrix membrane is treated with atmospheric plasma for efficient impregnation with C($100x'/x$)QPS-QPPO to increase the wettability of the hydrophobic matrix materials. The quality of the fabricated reinforced membrane is evaluated by scanning electron microscopy (SEM), and the mechanical, chemical, and electrochemical properties of the membranes are characterized by investigating the ion exchange capacity (IEC), the mechanical stability of the membranes using a universal testing machine (UTM), and the chemical stability by an *ex situ* soaking test, as well as the membrane area resistance, and the transport number. Moreover, in order to investigate the feasibility of the PErC($100x'/x$) QPS-QPPO membranes, five cell RED stacks with CMV/AMV (commercial cation/anion exchange membranes) or CMV/C($100x'/x$)QPS-QPPO are fabricated and compared with the commercial AMV membrane.[27,29]

2. Material and methods

2.1 Material

Chloroform, polystyrene (PS), poly(2,6-dimethyl-1,4-phenylene oxide) (PPO), 4,4′-diaminobenzophenone (DABP), *N*-bromosuccinimide (NBS), and trimethylamine solution were purchased from Sigma-Aldrich. *N*-Methylpyrrolidone (NMP), α,α'-azobisisobutyronitrile, Zinc chloride, and chloromethyl methyl ether were purchased from TCI. Chloromethylated polystyrene (cmPS) with a degree of chloromethylation of 0.55 was synthesized from polystyrene and brominated poly(2,6-dimethyl-1,4-phenylene oxide) (brPPO) with a degree of benzyl substitution of 0.35 [29–30]. Commercial cation and anion exchange membranes, *i.e.*, CMV and AMV (Selemion™), were purchased from Asahi Glass Co., Ltd. (Chiba, Japan). The porous polyethylene matrix membrane (thickness: 50 μm) was supplied by W-scope KOREA.

2.2 Synthesis of membrane

2.2.1. Synthesis of chloromethylated polystyrene (cmPS). Chloromethyl methyl ether (30.38 mL, 400 mmol) and zinc chloride (1.3 g, 9.6 mmol) were added to a stirred solution of 10 g of PS in chloroform (100 mL). The reaction mixture was subjected to reflux in an oil bath at the controlled temperature of 40 °C for 12 h, and the reaction mixture was added to a ten-fold excess of methanol to precipitate the product. After filtration, the polymer was dissolved in chloroform and reprecipitated in a methanol solution. The polymer was collected as a white powder and dried under vacuum at room temperature for one day (degree of chloromethylation: 55%). ^{1}H NMR ($CDCl_3$, δ ppm): Ar–CH_3 (1.2–1.8 ppm, m, 6H), Ar–CH_2–Cl (4.5 ppm, s, 2H), Ar–H of a PS repeat unit (6.5–7.1 ppm, m, 4H).[5,30]

2.2.2. Synthesis of brominated poly(2,6-dimethyl-1,4-phenylene oxide) (brPPO). NBS (14.76 g, 83 mmol) and AIBN (2.72 g, 16 mmol) were added to a stirred solution of 20 g of PPO in chlorobenzene (600 mL). The reaction mixture was subjected to reflux in an oil bath at the controlled temperature of 150 °C for 4 h, and the reaction mixture was added to a ten-fold excess of methanol to precipitate the product. After filtration, the polymer was dissolved in chloroform and reprecipitated in a methanol solution. The polymer was collected as a gray powder and dried under vacuum at 80 °C for one day (degree of bromination: 35%). ^{1}H NMR ($CDCl_3$, δ ppm): Ar–CH_3 (2.08 ppm, s, 9H), Ar–CH_2–Br (4.34 ppm, s, 2H), Ar–H of a PPO repeat unit (6.47 ppm, s, 2H), Ar–H of a bromomethylated PPO unit (6.5–6.7 ppm, m, 2H).[31,32]

2.2.3. Preparation of PE-reinforced membrane with cross-linked QPS-QPPO (PErC($100x'/x$)QPS-QPPO). The solute, which has a cmPS/brPPO mass ratio of 7 : 3, was dissolved in NMP, and different amounts (5, 10, and 15 mol% per total benzyl chloride of cmPS) of the cross-linker (DABP) were added to the mixed solution with a solid content of 10 wt%. Polyethylene film that was treated with atmospheric O_2 plasma for 10 s was immersed in the mixed solution for 30 min. The immersed PE membrane was dried on a vacuum plate for 30 min. The coated film was placed on a glass plate and dried in vacuum oven at 80 °C for 3 h. The PE-reinforced membranes with cross-linked cmPS-brPPO (PErC($100x'/x$)cmPS-brPPO) were peeled off from the glass plates and washed with deionized water. To introduce the quaternary ammonium groups as ion conducting groups, the membranes were placed into 1 M TMA,

as a quaternization reagent, in ethanol/acetone (50/50 vol%) for 12 h. After quaternization, the membranes were washed several times using acetone, and immersed in deionized water for 24 h. Based on the different amounts of cross-linker, the obtained anion conducting PE-reinforced cross-linked membranes are denoted as PErC(5)QPS-QPPO, PErC(10)QPS-QPPO, and PErC(15)QPS-QPPO, respectively.

2.3 Characterizations

Proton nuclear magnetic resonance (^{1}H NMR) spectroscopic measurements (Bruker DRX300 spectrometer at 300.13 MHz) were performed in $CDCl_3$ ($\delta = 7.28$ ppm) to study the chemical structures of the polymers. To investigate the ammonium group in the AEM, Fourier-transform infrared (FT-IR) spectra of the membranes were obtained in the range of 7500–375 cm^{-1} with a resolution of 2 cm^{-1} (Bruker ALPHA-P and ALPHA-T).

The ion exchange capacities (IEC, meq. g^{-1}) of the PErC(100x'/x)QPS-QPPO membranes were measured by the widely used titration method using an automatic titrator (Metrohm 794 Basic Titrino). The membranes were kept in a 1 M NaOH solution for 24 h. Subsequently, the membranes were immersed in 100 mL of 0.01 M HCl solution for 24 h. The remaining H^+ ions in solution were titrated with a 0.01 M NaOH solution. The IEC can be calculated from the following equation:

$$\text{IEC (meq. g}^{-1}) = \{C_{\text{NaOH}} \times (100 - V_{\text{NaOH}})\}/W_{\text{dry}} \quad (1)$$

where, C_{NaOH} is the concentration of NaOH solution (mol L^{-1}), V_{NaOH} is the volume of NaOH solution (L) used, and W_{dry} is the weight (g) of the dried membrane.

The water uptake was determined by weighing the membranes in the wet and dry conditions. First, the membrane sample (size: 2 cm × 2 cm) was immersed in de-ionized water at room temperature for 24 h for swelling. The membrane was subsequently wiped with a tissue paper and the wet weight (w_{wet}), length (l_{wet}), and thickness (t_{wet}) were measured. The sample was then dried under vacuum at 80 °C for 24 h. The different parameters were measured in the same manner as described above and the wet state was again determined by immersion in de-ionized water. The water uptake was calculated using the following equation:

$$\text{Water uptake (\%)} = (W_{\text{wet}} \times W_{\text{dry}})/W_{\text{dry}} \times 100 \quad (2)$$

The morphology of the membrane was investigated using a field-emission scanning electron microscope (FE-SEM, Vega ll LSU, TESCAN, Czech). Surface and cross-sectional images of the membranes were acquired for the dry membranes.

The proton conductivity of the membranes was measured by using an AC impedance analyzer (Solatron 1280, impedance/gain phase analyzer) in the temperature range of 25–40 °C under 100% relative humidity conditions along the in-plane direction over the frequency range of 0.1–20 kHz using a four-probe conductivity cell. The proton conductivity was calculated using the following equation:

$$\text{Proton conductivity (S cm}^{-1}) = l/(R \times S) \quad (3)$$

where l is the distance between the potential-sensing electrodes, S is the surface area measured for transporting a proton, and R is the impedance of the membrane.

Small-angle X-ray scattering (SAXS) measurements were used to characterize the morphologies of the synthesized membranes. SAXS analyses were performed using the PLS-II 3C beamline at the Pohang Accelerator Laboratory (PAL) in Korea. The scattering vector was calculated using the following equation:

$$q = 4\pi/\lambda \times \sin 2\theta \quad (4)$$

where q is the scattering vector, λ is the wavelength of the Cu Kα radiation ($\lambda = 1.542$ Å), and 2θ is the scattering angle. The inter-domain space (d) was calculated using the following equation:

$$d = 2\pi/q_{\max} \quad (5)$$

The mechanical properties of the dry membrane samples (1 × 7 cm^2) were measured with a universal testing machine (UTM) (model LR5K; LLOYD Co.) at room temperature. The crosshead speed was 10 mm min^{-1}. For accuracy, all measurements were performed in triplicate and averaged to get the final results.

The electrical resistance of the membranes was measured using a multi-meter (3560 AC mΩ HiTESTER, HIOKI. Ltd., Japanese). The membranes were immersed in 0.5 M NaCl aqueous solution for 24 h. The membrane was cut into 2 × 2 cm^2 squares and the electrical resistance of the membrane was measured at room temperature. The area resistance (AR) of the membrane was calculated according to the following equation:

$$\text{AR } (\Omega\ \text{cm}^2) = (R_2 - R_1) \times A \quad (6)$$

where R_2 is the electrical resistance of the membrane with 0.5 M NaCl aqueous solution, R_1 is the electrical resistance of 0.5 M NaCl aqueous solution, and A (0.1963 cm^2) is the effective area of the membrane.

The membrane transport number was determined by measuring the membrane potential. The cell had two compartments separated by the membrane that were circular in shape with an area of 4.0 cm^2. The membrane potential was measured by keeping the lower (0.001 M NaCl) to higher (0.005 M NaCl) salt concentration ratio constant. The potential difference (E_m) across the cell was measured using a multimeter (3560 AC mΩ HiTESTER, HIOKI. Ltd., Japanese) connected to Ag/AgCl reference electrodes that were responsive up to 0.10 mV. The transport number "t" was then calculated using the following modified Nernst equation:

$$E_m = RT/nF \times (2t - 1)\ln(C_1/C_2) \quad (7)$$

where, t is the transport number, E_m is the measured potential (V), R is the gas constant, T is the temperature (K), F is the Faraday constant, and C_1 and C_2 are the concentrations (mol L^{-1}) of the electrolyte solutions in the test cell.

The surface treatment was conducted using an atmospheric pressure plasma Levisystem apparatus. A 300 W 13.56 MHz RF discharge was ignited using a RF power supply (PTS PG0.313) through an impedance matcher (PTS PM0.313), which minimized the reflected power to under 1%. Both the outer surface of the plasma source body and the bottom moving table were electrically grounded. A stable homogeneous plasma discharge was obtained using 10 liters per minute of Ar. Oxygen gas (50 sccm) was added to the Ar plasma using mass flow controllers (MFC, AtoVac AFC500). The substrate was fixed on a moving table and the speed was set to 10 mm s^{-1} to treat the entire area of the mesh membrane for 10 s. The static contact angles were measured promptly by using a contact angle measuring instrument (SmartDrop, FemtoFab Ltd., Korea). For measurement of the water contact angle (WCA), a water droplet (12 μL) was automatically injected through a needle from a deionized water tank at 25 °C. Image analysis and contact angle computation were performed using drop-shape analysis software and assuming a circular profile of the droplet. The final data are the average of triplicate measurements to ensure accuracy.

The RED stack comprised two end plates (110 mm × 130 mm × 30 mm) made of acrylic resin and five cell pairs. Each cell pair contained a CEM, an AEM (effective area: 25 cm^2), and spacers (polyester mesh, South Korea). An additional CEM for shielding was located near the electrode to maintain the condition of the electrode compartment. Except for the shielding membrane, the membranes (CEMs and AEMs) were alternately stacked between the electrodes. The spacers were installed to provide a channel for the feed solutions. The electrodes (50 mm × 50 mm) were made of SUS 304 and were mechanically connected to platinized titanium current collectors (50 mm × 50 mm × 1.5 mm). An aqueous mixture of potassium hexacyanoferrate(II) and potassium hexacyanoferrate(III) (EP grade, Daejung, South Korea) (0.05 M) was used as the electrode solution and 0.5 M of sodium sulfate (EP grade, Daejung, South Korea) was used as the supporting electrolyte. Viton® tubing was used to prevent oxygen transfer to maintain the condition of the electrode solution. Artificial seawater (0.599 M NaCl) and river water (0.00856 M NaCl) were used as the feed solutions. To investigate the effect of the flow rate on the RED performance, the flow rates of the seawater and river water were equally changed from 10 to 100 mL min^{-1}, which corresponded to 2 to 20 mL per min per cell, respectively, and the change in the voltage (E) and current (I) with time was monitored. The gross power generation was calculated as the maximum value of the product of the voltage and current from the measured voltage–current curve. The gross power density was then calculated by dividing the corrected gross power generation by the total membrane effective area. The power density was measured *via* linear potential sweep using an electric load (PLZ164WA, Kikusui, Japan) at a sweep rate of 40 mV s^{-1}.

3. Results and discussion

3.1. Membrane characterization

3.1.1. FTIR, contact angle, and SEM. The procedure for evaluating the structures of PErC(100x'/x)QPS-QPPO and the embedded cross-linked ionomer structure is presented in Scheme 1. Synthesis of the polymer precursors with benzyl halides was confirmed by ^{1}H NMR analysis, as shown in Fig. S1.† The proton peaks of benzyl chloride and the chloromethyl group were observed at 6.5 ppm and 4.5 ppm, respectively, after chloromethylation of PS. The profile of brPPO also showed new peaks at 6.5–6.7 ppm and 4.3 ppm, which correspond to the proton peaks of benzyl bromide and the bromomethyl group, respectively. Moreover, there were no proton peaks at about 6.1 ppm, indicating that the side reaction was well-controlled in the bromination reaction. The conversion ratios (%) of the chloromethylation and bromination reactions were 55 and 35%, respectively.

For preparation of the reinforced membrane, the compatibility between the ionomers and PE matrix materials is a key factor for fabrication of high-quality membranes. Thus, before the impregnation and cross-linking step, as mentioned above, the porous PE matrix membrane (50 μm thick) was treated with atmospheric plasma under various conditions. As shown in Fig. 1, the measured contact angle of the porous PE matrix membrane was as high as 127° prior to surface treatment with the atmospheric plasma, indicating hydrophobicity of the matrix membrane surface. However, after surface treatment, the contact angle of the matrix membrane decreased considerably to 22–36°. The porous PE matrix membranes treated at output powers of over 150 W shrank in spite of the low contact angles. In this study, considering the power consumption and process time, all of the porous PE matrix membranes were treated at output powers of 90 W for 10 s.

After the *in situ* cross-linking process, PErC(100x'/x)cmPS-brPPO and PErC(100x'/x)QPS-QPPO were identified by FT-IR analysis, as shown in Fig. 2. The C=O stretching and C–N stretching vibration peaks were observed around 1690 cm^{-1} and 1100 cm^{-1} after the crosslinking reaction, respectively, indicating that the cross-linker successfully reacted with the alkyl halides on the precursor polymers (cmPS and brPPO).[33] The remaining alkyl halide groups on PErC(100x'/x)cmPS-brPPO were functionalized through a Menshutkin reaction to produce quaternary ammonium cations.[34] On quaternization, in order to facilitate penetration of the trimethylamine molecules into the membrane, the PErC(100x'/x)cmPS-brPPO membranes were swollen by immersion in a mixed EtOH : acetone solution of trimethylamine. After quaternization, a broad band around 3400 cm^{-1} corresponding to the OH vibration peak of water bound to quaternary ammonium cations was observed in the spectrum of PErC(100x'/x)QPS-QPPO, indicating successful fabrication of the PErC(100x'/x)QPS-QPPO membranes.[35,36]

The morphologies of the prepared PErC(100x'/x)QPS-QPPO membranes were studied by SEM. The surface and cross-sectional images were similar for all of the fabricated PErC(100x'/x)QPS-QPPO membranes.

Comparison of the surface SEM images of the PE matrix membrane and the PErC(5)QPS-QPPO membrane (Fig. 3(a) and (b)) with that of the reinforced ionomer membrane, PErC(5)QPS-QPPO, showed smooth surfaces without any defects. Moreover, as shown in Fig. 3(d–f), PErC(5)QPS-QPPO exhibited

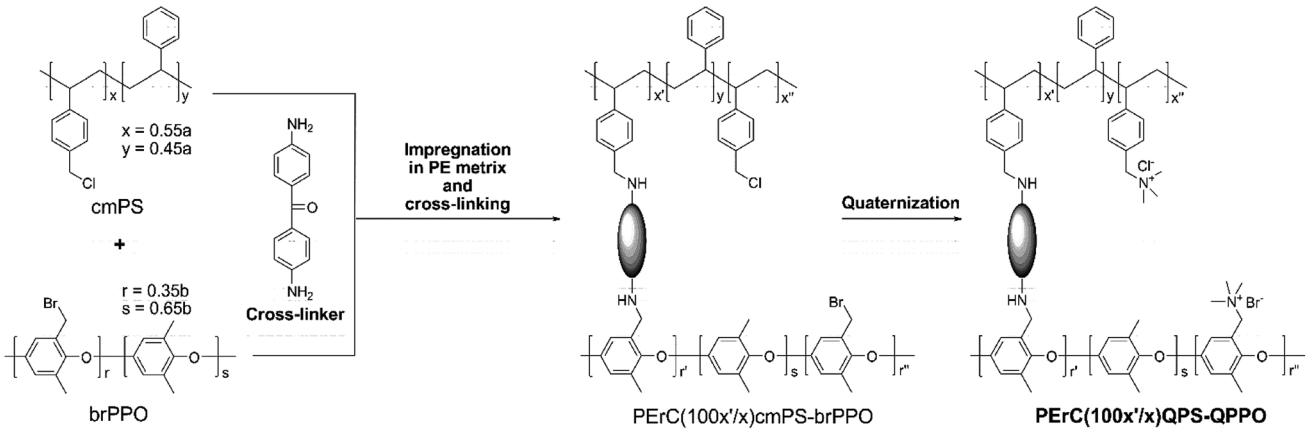

Scheme 1 Preparation of PE-reinforced anion exchange membrane based on cross-linked QPS-QPPO.

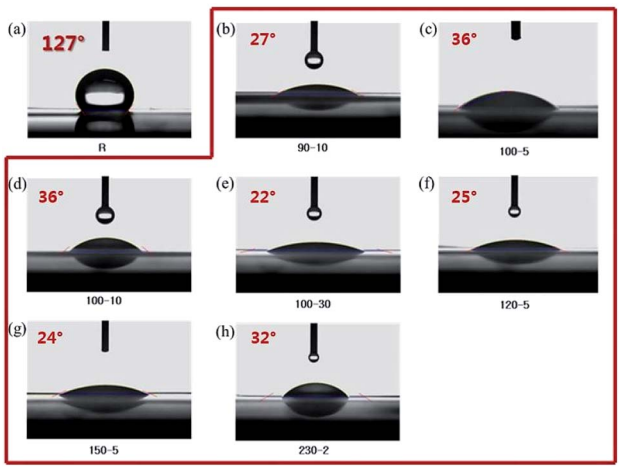

Fig. 1 Contact angles of non-treated PE matrix membrane (a) and PE matrix membrane treated with atmospheric plasma (b) at 90 W for 10 s, (c) at 100 W for 5 s, (d) at 100 W for 10 s, (e) at 100 W for 30 s, (f) at 120 W for 5 s, (g) at 150 W for 5 s, and (h) at 230 W for 2 s.

a dense inner structure in the cross-sectional image, indicating that the cross-linked ionomer was successfully embedded in the PE matrix membrane. The dense inner structure of the membrane should affect the cell resistance because the RED stack is composed of stacked CEMs and AEMs sandwiched between the electrodes. The inner structure of PErC(5)QPS-QPPO was notably dense without any pores, cracks, and vacancies, resulting from hydrophilic treatment of the PE matrix membrane using atmospheric plasma.

The nanoscale morphological property of the synthesized membrane material was investigated through SAXS analysis. In particular, PErC(5)QPS-QPPO was compared to C(5)QPS-QPPO, which was pristine ionomer membrane, for identifying nano-scale phase separation of the PErC(5)QPS-QPPO membrane. The average distance between the hydrophobic and hydrophilic clusters were investigated by the SAXS peak (q_{max}), as calculated using the Bragg equation in Fig. 4. Typically, random-structured ionomers indicate poor nano-scale phase separation morphology since the self-organization of the hydrophilic channel is not straightforward. In spite of the presence of a cross-linked random copolymer, the PErC(5)QPS-QPPO membrane indicated a phase-separated morphology in the SAXS profiles. The PErC(5)QPS-QPPO membrane showed two broad peaks at around 0.02 $Å^{-1}$ (d-spacing = 31 nm) and 0.028 $Å^{-1}$ (d-spacing = 22 nm), respectively. The diffraction peak at around 0.02 $Å^{-1}$ should originate from PE membrane, while another diffraction peak at around 0.028 $Å^{-1}$ resulted from embedded ionomer, that was C(5)QPS-QPPO, which

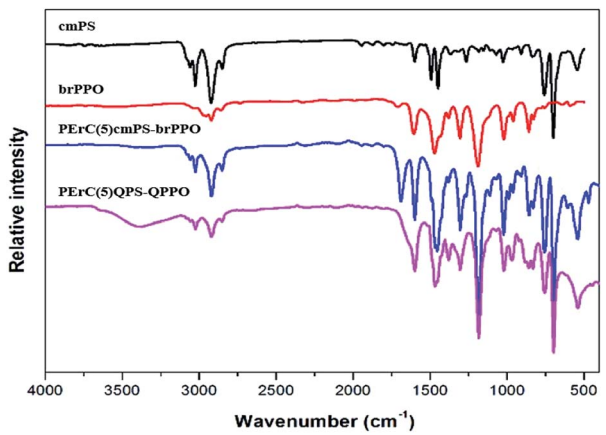

Fig. 2 ATR-FTIR spectrum of synthesized polymer and the fabricated membranes.

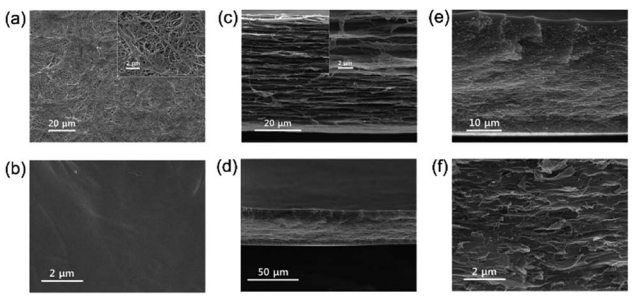

Fig. 3 Surface SEM images of (a) pristine PE (surface) and (b) PErC(5) QPS-QPPO membrane; cross-sectional SEM images of (c) pristine PE (cross section), and (d–f) PErC(5)QPS-QPPO membrane.

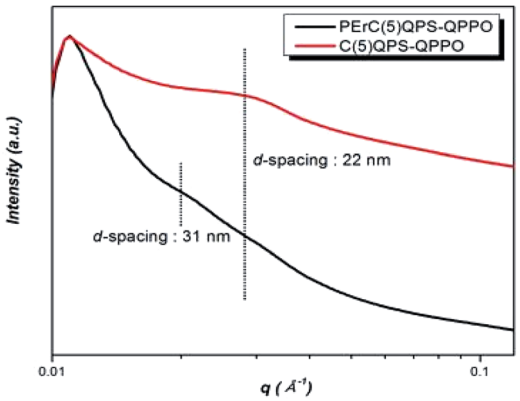

Fig. 4 SAXS profiles of PErC(5)QPS-QPPO and C(5)QPS-QPPO.

corresponded to the SAXS profile of pristine C(5)QPS-QPPO film. The clear ionomer peak of C(5)QPS-QPPO would stem from enhanced phase separation by cross-linking between different base polymers.

3.1.2. Physical, chemical, and electrochemical properties. The IEC is not only a fundamental property of IEMs, but is also a good indicator of the membrane resistance.[37] Typically, a higher IEC value corresponds to lower membrane resistance. However, because an excessively high IEC is associated with a decline in the chemical and mechanical properties of the membrane, an appropriate IEC value based on the nature of the matrix polymer is the most important consideration for IEM fabrication. As shown in Table 1, the IEC values of the fabricated membranes (1.0–1.2 meq. g^{-1}) were lower than that of the reference membrane (AMX), due to the porous PE matrix membrane. That is, although the ion exchange polymer material showed a very high IEC, the reinforced IEMs exhibited low IEC values because the porous PE matrix membrane does not have ion exchange groups. The IEC values of the cross-linked membranes decreased with an increase in the degree of cross-linking because an equivalent amount of cross-linking and benzyl halide groups on cmPS and brPPO was consumed in the cross-linking reaction.

The water uptake (WU), which is dependent on the IEC, the nature of the ionomer, and the morphology and acidity of the ion exchanged groups, is regarded as another key factor influencing the membrane resistance and electrochemical properties. Typically, the WU increases with an increase in the IEC, which leads to an increase in the ion conductivity because the water molecules in the IEM facilitate ion transport by forming ion transport channels. As shown in Fig. 5, the WUs of the PErC(100x'/x)QPS-QPPO membranes decreased with an increase in the degree of cross-linking. Compared to AMV, PErC(10)QPS-QPPO and PErC(15)QPS-QPPO showed lower WUs of 25% and 20%, respectively. Although PErC(5)QPS-QPPO exhibited the highest WU (37%) among the fabricated membranes, this WU is still considered low. Despite the higher IEC, the WU of AMV was lower than that of PErC(5)QPS-QPPO, which may be derived from the high cross-linking degree of AMV.

The area resistance of the IEM is a key electrochemical parameter for REDs, as the total cell current is closely related to the total cell resistance, which is considerably influenced by the membrane resistance. The electrical resistance of the membranes was measured *via* the two-probe method using a home-made measurement cell with platillized platinum electrodes. The membranes were equilibrated with 0.5 M NaCl aqueous solution over one day. After pouring the 0.5 M NaCl aqueous solution into the two compartments of the cell, the internal electrical resistance of the cell without the membrane was measured using an LCR meter at 1 kHz at room temperature. The electrical resistance of the cell with the membrane was then measured under the same conditions. The difference between the electrical resistance of the cell with the membrane and that without the membrane is the electrical resistance of the membrane. The area resistance was calculated from the electrical resistance and active area of the membrane.

As shown in Table 1, the area resistance increased with an increase in the degree of cross-linking; nevertheless, the area resistance of all the prepared membranes was lower (0.69–1.67

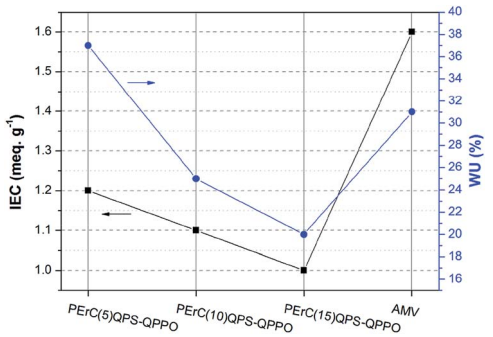

Fig. 5 Comparison of IEC and WU of developed membranes and AMV.

Table 1 Comparison of various properties of fabricated membranes *versus* AMV

Membranes	Thickness (μm)	IEC (meq. g^{-1})	Water uptake (%)	Area resistance (Ω cm^2)	Conductivity (mS cm^{-1}) 25 °C	Conductivity (mS cm^{-1}) 40 °C	Transport number (%)
PErC(5)QPS-QPPO	51	1.2	37	0.69	3.1	4.1	96
PErC(10)QPS-QPPO	46	1.1	25	1.33	2.8	4.2	96
PErC(15)QPS-QPPO	40	1.0	20	1.67	3.0	4.1	97
AMV	150	1.6	31	2.58	1.1	1.5	97

Ω cm^2) than that of AMV (2.58 Ω cm^2). Even when a relatively thin fabricated membrane was considered (PErC(5)QPS-QPPO), the membrane resistance was low, being only about a quarter of that of AMV. The low area resistance of the fabricated membranes is expected to lead to enhancement of the RED performance as the membrane resistance accounts for a large portion of the total cell resistance. Interestingly, although PErC(5)QPS-QPPO showed a lower IEC than AMV, the WU was higher and the membrane resistance of the former was lower, which could stem from the different base polymer structures.

In the RED system, the salinity gradient leads to a potential difference, which is approximately 80–100 mV for seawater and river water. Typically, the cell potential increases with an increase in the concentration difference between the concentrated salt solution and dilute salt solution, as well as with an increase in the transport number of the IEMs. The membrane resistance and transport number are highly influenced by the IEC; that is, increasing the IEC leads to a decrease in the membrane resistance and transport number as membranes with a high IEC can transport counter-ions more effectively, but the permselectivity between the co-ion and the counter-ion may be lowered. As shown in Table 1, the transport numbers of the fabricated membranes increased with an increase in the degree of cross-linking, which stemmed from the decrease in the IEC. Despite the considerable thinness of the membrane relative to that of AMV, the fabricated membranes showed outstanding transport numbers of over 0.96, which are comparable to those of commercial AMV membranes. Considering that the generated electromotive force (EMF) is affected by the permselectivity of the membranes, it was expected that the output potentials of the RED stacks with the fabricated membranes would be comparable to that of the RED stack with the AMV membrane.

3.1.3. Mechanical properties and chemical stability. The fabricated membranes showed outstanding mechanical properties in an analytical experiment employing the UTM (Fig. S3†). The tensile strength (29–43 MPa) and elongation at break (7–13%) of all the fabricated membranes were higher than those of AMV under 50% relative humidity (R.H.) conditions, which should originate not only from the polymer main chain structure, but also the physical properties of the supporting PE membrane. The tensile strength increased with an increase in the degree of cross-linking (Table 2).

The chemical stability is a significantly important property; in particular, the alkaline stability is a critical parameter for judging the chemical stability of AEMs as the quaternary ammonium groups of AEMs are easily degraded under basic conditions. The membranes were immersed in 2 M NaOH solution at room temperature for 250 h, and the variations in the IEC over time were investigated.[29,43,44]

Because the alkaline stability typically decreases with an increase in the WU, higher alkaline stability of AMV was expected relative to that of PErC(5)QPS-QPPO that had a higher WU. However, the expectation did not correspond with the experimental results. As shown in Fig. 6, compared to the initial IEC values, after 250 h of testing, the IEC retention of the fabricated membranes, PErC(5)QPS-QPPO, PErC(10)QPS-QPPO, and PErC(15)QPS-QPPO, was as high as 75, 77, and 81%, respectively, where these values are higher than that of AMV (70%). Comparison of PErC(5)QPS-QPPO and AMV showed that although PErC(5)QPS-QPPO had a cross-linking degree as low as 5 mol%, its IEC retention was higher than that of AMV, which should stem from the difference in the magnitude of the WU. In addition, the nature of the embedded ionomer materials, as well as the amount of ionomer in the reinforced membrane, should affect the chemical stability of the membranes.

3.2. Performance of membranes in RED stack

The power generation of PErC(5)QPS-QPPO and that of the commercial AMV membranes was tested in a RED stack by using CMV membranes as the CEMs. The complete results are presented in Fig. S4 and S5.† At least three measurements were conducted for each AEM, and the average values are reported. The open circuit voltages (OCV) of the RED stacks with the PErC(5)QPS-QPPO and AMV membranes as AEMs were evaluated as function of the linear flow rate of the feed solution (Fig. 7(a)). In general, the OCV is influenced by the permselectivity of the IEMs, co-ions, counter-ions, temperature, and concentration difference between the concentrated and dilute solutions. In particular, assuming that the temperature and concentration difference are constant and the dissolved ions are Na^+ and Cl^-, the permselectivity of the IEM is considered to be the most crucial factor affecting the OCV. According to the Nernst equation, the theoretical OCV of a five cell-pair stack with 100% permselective membranes is equal to 1.09 V at 25 °C when saline solutions are used.

The OCV values of the two stacks with the PErC(5)QPS-QPPO and AMV membranes, respectively, increased with an increase in the flow rate of the feed solution, but became saturated at flow rates exceeding 60 mL min^{-1}. The low OCV values at low flow rates resulted from the concentration polarization in the vicinity of the membrane surface, caused by less efficient solution mixing.[35,38–40] Moreover, the cations and anions have longer residence times in each compartment cell at lower flow rates, which gives rise to a decrease in the salt concentration gradient between the two saline streams flowing along the respective channels. Compared to the theoretical value, the experimental OCVs of the two stacks with the PErC(5)QPS-QPPO and AMV membranes were 75.4–78.7% and 76.6–81.5%,

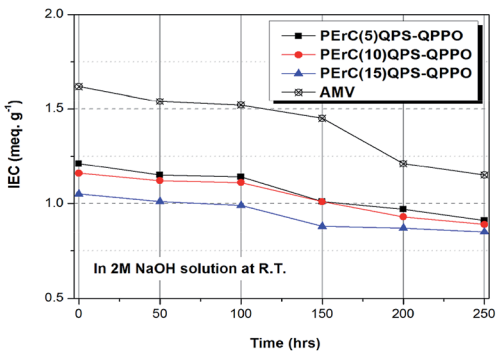

Fig. 6 Comparison of the chemical stability of fabricated membranes *versus* AMV in 2 M NaOH solution at 25 °C.

Table 2 Comparison of mechanical properties of fabricated membranes and AMV

	Mechanical property		
Membranes	Young's modulus (GPa)	Tensile strength (MPa)	Elong. at break (%)
PErC(5)QPS-QPPO	1.43	29	13
PErC(10)QPS-QPPO	1.44	32	7
PErC(15)QPS-QPPO	1.46	43	10
AMV	1.52	19	4

respectively. As shown in Fig. 7(a), the RED stack with the PErC(5)QPS-QPPO membrane had a lower OCV than that with the AMV membrane, which may originate from the lower permeability and low membrane thickness. Nevertheless, the RED stack with the PErC(5)QPS-QPPO membrane exhibited an outstanding OCV as high as 0.86 V at flow rates over 60 mL min^{-1}, where this value is only 0.03 V lower than that with the AMV membrane.

Another key factor determining the output power of the RED stack is the short circuit current (SSC). As mentioned above, the fabricated PErC(5)QPS-QPPO membrane was thinner than the AMV membrane, resulting in lower membrane resistance. The internal resistance of the RED stack is one of the core parameters determining its SSC. Typically, the total internal resistance is derived from the AEM and CEM membranes, the high salinity and low salinity compartments, and the electrodes.[41–43] Considering that the membrane resistance accounts for the major part of the total internal resistance, it was expected that the RED stack with the PErC(5)QPS-QPPO membrane would exhibit outstanding SSC properties, superior to that with the AMV membrane. As shown in Fig. 7(b), the short circuit current of the RED stack with the PErC(5)QPS-QPPO membrane was much higher than that with the AMV membrane over the entire flow rate range. In particular, at the high flow rate of 100 mL min^{-1}, the RED stack with the PErC(5)QPS-QPPO membrane showed an outstanding SSC value, as high as 0.212 A, which is 25.4% higher than that (0.169 A) of the RED stack with the AMV membrane. The outstanding SSC of the RED stack with the PErC(5)QPS-QPPO membrane may be derived from the higher anion conductivity and lower area resistance, which originate from the thinness of the PErC(5)QPS-QPPO membrane relative to that of the AMV membrane. The difference in the short circuit current of the two stacks increased with an increase in the flow rate, as a high flow rate leads to greater ion flux by decreasing the concentration polarization.

The maximum power densities (MPD) of the two RED stacks with the PErC(5)QPS-QPPO and AMV membranes, respectively, were compared as a function of the flow rate (Fig. 7(c)). Like the SSC values, the MPD value of the RED stack with the PErC(5) QPS-QPPO membrane increased with increasing flow rate, and was much higher than that of the RED stack with the AMV membrane over the entire flow rate range. The excellent MPD resulted from the outstanding SSC value. That is, although the OCV of the RED stack with the PErC(5)QPS-QPPO membrane was slightly lower, the SSC was much higher than that of the RED stack with the AMV membrane. The RED stack with the PErC(5)QPS-QPPO membrane showed an outstanding MPD value of 1.82 W m^{-2} at a flow rate of 100 mL min^{-1}, which is 20.7% higher than that (1.50 W m^{-2}) of the RED stack with the AMV membrane. Moreover, the RED stack with the PErC(5)QPS-QPPO membrane exhibited similar rates of increase in the MPD value, *i.e.*, around 20%, even at flow rates lower than 100 mL min^{-1}. The MPD was 26.3, 19.2, 18.4, 20.0, 20.9, and 20.7% at 10, 20, 40, 60, 80, and 100 mL min^{-1}, respectively. Considering that the RED system cannot be commercially used without taking the power density and price into account, the PErC(5) QPS-QPPO membrane is a promising candidate for REDs due to its outstanding cell properties, low material cost, and facile fabrication process.

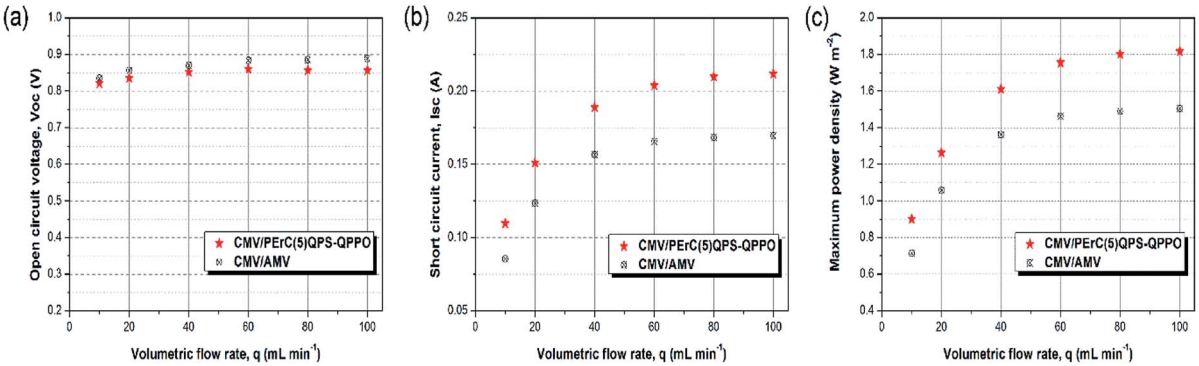

Fig. 7 Comparison of OCV, SSC, an MPD as a function of the flow rate for the RED stacks.

4. Conclusions

With the aim to fabricate AEMs with high efficiency and reasonable cost for REDs, the low-cost materials, PS and PPO, were introduced into the backbone of ionomers. Moreover, the ionomers were cross-linked with a diamine-based cross-linker to improve their physical stability. Furthermore, the ionomers were impregnated into a PE matrix support to maximize the mechanical properties. Before impregnation with the ionomers, the porous PE matrix membrane was treated with atmospheric plasma to achieve efficient impregnation of CQPS-QPPO by increasing the compatibility between the ionomer and the matrix membrane. Consequently, PE-reinforced AEMs based on cross-linked QPS-QPPO were successfully fabricated. PErC(5) QPS-QPPO showed the optimal electrochemical properties for use in the RED. The membrane resistance was much lower than that of the commercial AEM (AMV). Despite the thinness of the film, the transport number of PErC(5)QPS-QPPO was comparable to that of AMV, and the former also showed outstanding chemical stability in an acceleration test. The RED stack with the PErC(5)QPS-QPPO membrane showed an outstanding MPD of 1.82 W m^{-2} at a flow rate of 100 mL min^{-1}, which is 20.7% higher than that (1.50 W m^{-2}) of the RED stack with the AMV membrane. These results suggest that the PErC(5)QPS-QPPO membrane is a promising candidate for use in RED systems as an alternative AEM to AMV.

Conflicts of interest

There are no conflicts to declare.

Acknowledgements

This work was supported by the Technology Innovation Program (10047796, Cation/Anion Exchange and Adsorption Polymers for Desalination Applications) funded by the Ministry of Trade, Industry, and Energy (MOTIE) of the Republic of Korea.

Notes and references

1 J. Ran, L. Wu, Y. He, Z. Yang, Y. Wang, C. Jiang, L. Ge, E. Bakangura and T. Xu, *J. Membr. Sci.*, 2017, **522**, 267–291.
2 S. Zhu, R. S. Kingsbury, D. F. Call and O. Coronell, *J. Membr. Sci.*, 2018, **554**, 39–47.
3 B. Kang, H. J. Kim and D. K. Kim, *J. Membr. Sci.*, 2018, **550**, 286–295.
4 D. H. Cho, K. H. Lee, Y. M. Kim, S. H. Park, W. H. Lee, S. M. Lee and Y. M. Lee, *Chem. Commun.*, 2017, **53**, 2323–2326.
5 M. S. Cha, H. Y. Jeong, H. Y. Shin, S. H. Hong, T. H. Kim, S. G. Oh, J. Y. Lee and Y. T. Hong, *J. Power Sources*, 2017, **363**, 78–86.
6 N. Y. Yip, D. Brogioli, H. V. Hamelers and K. Nijmeijer, *Environ. Sci. Technol.*, 2016, **50**, 12072–12094.
7 M. Wang, X. Xu, Y. Li, T. Lu and L. Pan, *Desalination*, 2018, **443**, 221–227.
8 E. Güler, R. Elizen, D. A. Vermaas, M. Saakes and K. Nijmeijer, *J. Membr. Sci.*, 2013, **446**, 266–276.
9 G. Amy, N. Ghaffour, Z. Li, L. Francisc, R. V. Linaresc, T. Missimerd and S. Lattemann, *Desalination*, 2017, **401**, 16–21.
10 H. Zhang, D. Jiang, B. Zhang, J. G. Hong and Y. Chen, *Electrochim. Acta*, 2017, **239**, 65–73.
11 C. Klaysom, S. H. Moon, B. P. Ladewig, G. Q. M. Lu and L. Z. Wang, *J. Membr. Sci.*, 2011, **371**, 37–44.
12 T. Luo, S. Abdu and M. Wessling, *J. Membr. Sci.*, 2018, **555**, 429–454.
13 C. Klaysom, R. Marschall, S.-H. Moon, B. P. Ladewig, G. Q. M. Lu and L. Wang, *J. Mater. Chem.*, 2011, **21**, 7401–7409.
14 A. H. Avci, R. A. Tufa, E. Fontananova, G. D. Profio and E. Curcio, *Energy*, 2018, **165**, 512–521.
15 T. W. Xu, *J. Membr. Sci.*, 2005, **263**, 1–29.
16 M. I. Khan, C. Zheng, A. N. Mondal, M. M. Hossain, B. Wu, K. Emmanuel, L. Wu and T. Xu, *Desalination*, 2017, **402**, 10–18.
17 L. Wu, T. W. Xu and W. Yang, *J. Membr. Sci.*, 2006, **286**, 185–192.
18 C. C. Yang, S. J. Chiu, W. C. Chien and S. S. Chiu, *J. Power Sources*, 2010, **195**, 2212–2219.
19 T. W. Xu, D. Wu and L. Wu, *Prog. Polym. Sci.*, 2008, **33**, 894–915.
20 J. Pan, J. Ding, R. Tan, G. Chen, Y. Zhao, C. Gaoa, B. V. Bruggen and J. Shen, *J. Membr. Sci.*, 2017, **539**, 263–272.
21 X. Li, Q. Liu, Y. Yu and Y. Meng, *J. Mater. Chem. A*, 2013, **1**, 4324–4335.
22 Q. H. Zeng, Q. L. Liu, I. Broadwell, A. M. Zhu, Y. Xiong and X. P. Tu, *J. Membr. Sci.*, 2010, **349**, 237–243.
23 S. Yun, H. Im, Y. Heo and J. Kim, *J. Membr. Sci.*, 2011, **380**, 208–215.
24 A. Zlotorowicz, R. V. Strand, O. S. Burheim, Ø. Wilhelmsen and S. Kjelstrup, *J. Membr. Sci.*, 2017, **523**, 402–408.
25 M. Tedesco, H. V. M. Hamelers and P. M. Biesheuvel, *J. Membr. Sci.*, 2017, **531**, 172–182.
26 M. Tedesco, A. Cipollina, A. Tamburini and G. Micale, *J. Membr. Sci.*, 2017, **522**, 226–236.
27 D. R. Dekel, M. Amar, S. Willdorf, M. Kosa, S. Dhara and C. E. Diesendruck, *Chem. Mater.*, 2017, **29**, 4425–4431.
28 J. Choi, S. C. Yang, N. J. Jeong, H. Kim and W. S. Kim, *Langmuir*, 2018, **34**, 10837–10846.
29 M. I. Khan, A. N. Mondal, B. Tong, C. Jiang, K. Emmanuel, Z. Yang, L. Wu and T. Xu, *Desalination*, 2016, **391**, 61–68.
30 A. Yovani, L. Bermúdez and R. Salazar, *CT&F, Cienc., Tecnol. Futuro*, 2008, **3**, 157–167.
31 H. I. Chang, M. S. Yang and M. Liang, *React. Funct. Polym.*, 2010, **70**, 944–950.
32 A. L. Ong, S. Saad, R. Lan, R. J. Goodfellow and S. Tao, *J. Power Sources*, 2011, **196**, 8272–8279.
33 Q. Zhang, Q. Zhang, S. Zhang and S. Li, *J. Membr. Sci.*, 2010, **354**, 23–31.
34 S. Diao, F. Dong, J. Meng, P. Ma, Y. Zhao and S. Feng, *Mater. Chem. Phys.*, 2015, **153**, 161–167.

35 H.-K. Kim, M.-S. Lee, S.-Y. Lee, Y.-W. Choi, N.-J. Jeong and C.-S. Kim, *J. Mater. Chem. A*, 2015, **3**, 16302–16306.
36 M. S. Cha, J. Y. Lee, T. H. Kim, H. Y. Jeong, H. Y. Shin, S. G. Oh and Y. T. Hong, *J. Membr. Sci.*, 2017, **530**, 73–83.
37 H. Y. Shin, M. S. Cha, S. H. Hong, T. H. Kim, D. S. Yang, S. G. Oh, J. Y. Lee and Y. T. Hong, *J. Mater. Chem. A*, 2017, **5**, 12285–12296.
38 D. A. Vermaas, M. Saakes and K. Nijmeijer, *J. Membr. Sci.*, 2011, **385**, 234–242.
39 J. Veerman, M. Saakes, S. J. Metz and G. J. Harmsen, *J. Membr. Sci.*, 2009, **327**, 136–144.
40 P. Długołecki, K. Nymeijer, S. Metz and M. Wesslinga, *J. Membr. Sci.*, 2008, **319**, 214–222.
41 J. Veerman, R. M. de Jong, M. Saakes, S. J. Metz and G. J. Harmsen, *J. Membr. Sci.*, 2009, **343**, 7–15.
42 J. Veerman, J. W. Post, M. Saakes, S. J. Metz and G. J. Harmsen, *J. Membr. Sci.*, 2008, **310**, 418–430.
43 F. Liu, O. Coronell and D. F. Call, *J. Power Sources*, 2017, **355**, 206–210.
44 J. G. Hong, B. Zhang, S. Glabman, N. Uzal, X. Dou, H. Zhang, X. Wei and Y. Chen, *J. Membr. Sci.*, 2015, **486**, 71–88.